Available online at website: https://journal.bcrec.id/index.php/bcrec

Bulletin of Chemical Reaction Engineering & Catalysis, 21 (3) 2026, 737-748

Original Research Article

ZIF-67 Incorporated Sodium Alginate/Polyvinyl Alcohol Composite Beads for Efficient Adsorptive Removal of Reactive Blue 19 from Aqueous Solution

Nguyen Thi Hong Nhung[1], Pham Thi Huynh Nhu[1], Hoang Ai Le Pham[1], Thi Hong Anh Nguyen[2,*]

[1]Faculty of Chemical Engineering, Industrial University of Ho Chi Minh City, 12 Nguyen Van Bao Rd, Ho Chi Minh City 700000, Viet Nam.
[2]Faculty of Chemical Engineering, Ho Chi Minh City University of Industry and Trade, 140 Le Trong Tan Street, Tay Thanh Ward, Ho Chi Minh City 700000, Viet Nam.

Received: 20th May 2026; Revised: 27th June 2026; Accepted: 27th June 2026
Available online: 30th June 2026; Published regularly: October 2026

Abstract

In this study, ZIF-67/SA/PVA composite beads were synthesized and used to remove Reactive Blue 19 (RB19) from aqueous solution. The composites were prepared by integrating cobalt-based ZIF-67 into a sodium alginate/polyvinyl alcohol matrix with different SA/PVA ratios. The physicochemical properties of the composites were characterized by FT-IR, XRD, SEM–EDS, BET, TG, and pH_{pzc} analyses. Among the investigated samples, ZIF-67/SA/PVA-1:3 exhibited the highest RB19 removal efficiency (96.45%). The removal efficiency increased with increasing adsorbent dosage and temperature, but decreased at higher RB19 concentrations. The pH-dependent adsorption behavior was consistent with the pH_{pzc} of 7.77. The negative $\Delta G°$ values (−5.308 to −7.298 kJ.mol^{-1}) and the positive $\Delta H°$ value of 15.297 kJ.mol^{-1} indicated that the adsorption process was spontaneous and endothermic. The equilibrium data fitted the Langmuir model better than the Freundlich model. These findings demonstrate the potential of ZIF-67/SA/PVA as a composite adsorbent for removing reactive dyes from contaminated water.

Keywords: ZIF-67; sodium alginate; polyvinyl alcohol; Reactive Blue 19; wastewater treatment

How to Cite: Nhung, N. T. H., Nhu, P. T. H., Pham, H. A. L., Nguyen, T. H. A. (2026). ZIF-67 Incorporated Sodium Alginate/Polyvinyl Alcohol Composite Beads for Efficient Adsorptive Removal of Reactive Blue 19 from Aqueous Solution. *Bulletin of Chemical Reaction Engineering & Catalysis*, 21 (3), 737-748. (DOI: 10.9767/bcrec.20747)

Permalink/DOI: https://doi.org/10.9767/bcrec.20747

1. Introduction

The rapid expansion of the textile industry has led to large-scale discharge of dye-containing wastewater into aquatic environments. Among various classes of dyes, reactive dyes are of particular concern because of their high chemical stability, resistance to biodegradation, and potential toxicity even at low concentrations [1,2]. Reactive blue 19 (RB19) is an anthraquinone-based dye widely used for dyeing cellulosic fibers. Approximately 20–25% of the applied dye may be released into wastewater streams. Moreover, RB19 exhibits remarkable persistence in natural environments with a half-life exceeding 40 years. This causes long-term ecological and human health risks. Previous studies have shown that textile dyes can adversely affect aquatic organisms and harm embryonic development in marine species. Accordingly, the development of efficient, cost-effective and environmentally benign treatment technologies is increasingly important [3]. Among available treatment methods, adsorption has gained considerable attention because of its operational simplicity, high efficiency, and adaptability [4].

Sodium alginate (SA) has been widely used in biomedical, food, and environmental applications because of its biocompatibility, biodegradability, and low toxicity. SA hydrogel-based adsorbents exhibit strong affinity for heavy metals and

* Corresponding Authors.
Email: anhnth@huit.edu.vn (T.H.A. Nguyen)

organic dyes because they contain the abundant carboxylate (–COO^-) and hydroxyl (–OH) groups. These functional groups enable electrostatic attraction, ion exchange, and hydrogen bonding. However, pristine SA has several inherent limitations, including low mechanical strength, poor stability in aqueous media, and limited adsorption capacity [5–7]. These limitations restrict its practical application in the removal of synthetic dyes and antibiotics. To address these drawbacks, the fabrication of SA-based composites has become an effective approach for improving structural stability and introducing additional adsorption sites [8,9]. Especially, the incorporation of nanomaterials and microparticles into SA matrices has been found to significantly improve adsorption performance and separability [10–12].

Metal–organic frameworks (MOFs) have attracted considerable attention because of their high surface areas, tunable pore structures, and versatile chemical functionalities [13–16]. ZIF-67 is a cobalt-based zeolitic imidazolate framework constructed from Co^{2+} ions and 2-methylimidazole ligands. Its high crystallinity, microporous structure, and affinity for organic molecules make ZIF-67 a promising material for the adsorption-based removal of contaminants from water [17]. In addition to adsorption, ZIF-67-based composites have been investigated for membrane filtration and catalytic oxidation. For example, ZIF-67-based membranes coupled with peroxymonosulfate activation have achieved high removal efficiencies for organic dyes. Nevertheless, incorporating ZIF-67 into polymer matrices enhances the separability of the treated materials. However, ZIF-67 suffers from limitations in poor mechanical stability, particle aggregation, and difficulty in separation from aqueous systems. To overcome these limitations, hybridization of ZIF-67 with polymer matrices has been widely explored. In this context, combining SA with polymers, such as polyvinyl alcohol [18], melamine [19], and cellulose [20], yields a robust, flexible polymeric network. These combinations showed the good adsorption properties due to the strong hydrogen bonding interactions between the functional group of the polymer and the –COO^- and –OH groups of SA. The incorporation of ZIF-67 into these matrices can therefore integrate the adsorption sites with the structural support and processability of the polymer network. Although substantial progress has been made in MOF–polymer composites, studies of ZIF-67/SA/PVA bead systems for reactive dye removal remain limited [18]. Although significant progress has been made in the development of MOF-based composites, studies on ZIF-67/SA/PVA systems for the removal of reactive dyes from textile wastewater remain relatively limited. Most previous works have focused on powder-form MOFs or simple polymer blends with poor recyclability and limited applicability in continuous systems [19]. The study aimed to develop ZIF-67/SA/PVA composite beads that address key limitations associated with powder-form MOF adsorbents, including particle aggregation, poor mechanical integrity, and difficulty separating from aqueous media. The composite combines the microporous adsorption sites of the ZIF-67 with the structural stability of SA/PVA network. More importantly, this work establishes a clear relationship between the SA/PVA composition, physicochemical properties, and RB19 adsorption behavior that provide useful design principles for optimizing MOF/polymer hybrid adsorbents. The resulting composite beads exhibit high RB19 removal efficiency under mild operating conditions and can be readily separated from the treated solution. This study demonstrated the potential of this adsorbent platform for the treatment of dye-contaminated wastewater.

2. Materials and Methods

2.1 Materials

Sodium alginate (98%), polyvinyl alcohol, calcium chloride, methanol, 2-methylimidazole, and cobalt(II) nitrate hexahydrate were obtained from Sigma-Aldrich Chemical Co and used as received without further purification. Reactive blue 19 (CAS No. 2580-78-1) was obtained from Thanh Cong Textile Dyeing Company (Viet Nam) with a stated purity of 98% and was used without further purification.

2.2 Synthesis of ZIF-67/SA/PVA Composites

Sodium alginate (0.5 g) was dissolved in 10 mL of distilled water under continuous stirring for 8 h. Separately, 0.5 g of polyvinyl alcohol was dissolved in 10 mL of distilled water. The PVA solution was then added dropwise to the SA solution under continuous stirring at 85 °C for 1 h to obtain a homogeneous blend. The resulting mixture was injected dropwise into a 0.3 M $CaCl_2$ solution using a syringe pump with continuous stirring to deliver uniform spherical beads. The beads were aged in a $CaCl_2$ solution for 1 h and washed with distilled water to remove excess $CaCl_2$. Separately, 0.652 g of $Co(NO_3)_2 \cdot 6H_2O$ was dissolved in 50 mL of methanol in a 100 mL beaker under continuous stirring. The pre-washed beads were then immersed in $Co(NO_3)_2$ solution, followed by the addition of 1.471 g of 2-methylimidazole (Co^{2+}:ligand molar ratio = 1:8). The reaction was allowed to proceed at room temperature for 6h. The obtained beads were thoroughly washed with distilled water until the pH was 7. The beads were freeze-dried for 12 h to obtain purple ZIF-67/SA/PVA-1:1 composite

beads. The same procedure was applied using 0.25 g SA and 0.75 g PVA or 0.75 g SA and 0.25 g PVA to obtain ZIF-67/SA/PVA-1:3 and ZIF-67/SA/PVA-3:1, respectively. The numerical designations refer to the SA:PVA mass ratio.

2.3. Adsorption Experiments

Batch adsorption experiments were conducted to evaluate the RB19 removal by ZIF-67/SA/PVA composites. All experiments were performed using 50 mL of RB19 solution in 100 mL Erlenmeyer flasks under agitation at 250 rpm. Unless otherwise stated, 0.1 g of ZIF-67/SA/PVA composite was added to a 30 mg/L RB19 solution. At predetermined time intervals, 4 mL aliquots were withdrawn, separated from the adsorbent, and analyzed by UV–Vis spectrophotometry over the wavelength range of 450–750 nm. The effects of SA/PVA mass ratio, adsorbent dosage, initial RB19 concentration, solution pH, and temperature were systematically investigated. All experiments were conducted in triplicate. The removal efficiency and adsorption capacities were calculated using Eqs. (1)-(3).

$$q_t = \frac{(C_0 - C_t)\,V}{m} \quad (1)$$

$$q_e = \frac{(C_0 - C_e)\,V}{m} \quad (2)$$

$$Removal\ (\%) = \frac{(C_0 - C_t)}{C_0} \times 100\% \quad (3)$$

where: q_t (mg.g^{-1}) is the adsorption capacity at time t, q_e (mg.g^{-1}) is the adsorption capacity at equilibrium. C_0, C_t, and C_e (mg.L^{-1}) are the initial, time t, and equilibrium concentrations of RB19, respectively, V (L) and m (g) are the solution volume and the adsorbent mass, respectively.

The effect of SA/PVA polymer composition was studied with different SA:PVA weight ratios (3:1, 1:1, and 1:3). For each experiment, 0.1 g of the ZIF-67/SA/PVA composite was added to 50 mL of a 30 mg/L RB19 solution. The adsorption experiment was monitored over time intervals ranging from 0 to 210 min. The effect of initial RB19 concentration was studied at 20-60 mg/L and 0.1 g of the ZIF-67/SA/PVA-1:3 composite. The adsorption process was monitored over time up to 480 min. Additionally, the effect of adsorbent dosage was carried out at 0.05, 0.075, 0.10, and 0.20 g of composite. The effect of solution pH was investigated by adjusting the initial pH of 5 to 9.

2.4. Determination of the Point of Zero Charge

The point of zero charge (pH_{pzc}) was determined by adding 0.1 g of adsorbent to 50 mL of 0.1 M NaCl solution with initial pH values from 4 to 9. The resulting suspensions were shaken at 250 rpm for 24 h. The final pH (pH_f) was recorded, and $\Delta pH = pH_f - pH_i$ was calculated. The pH_{pzc} was determined as the point at which $\Delta pH = 0$.

2.5. Thermodynamic Analysis

The effect of temperature was evaluated at 303, 313, 323, and 333 K using 0.1 g of ZIF-67/SA/PVA-1:3 in 50 mL of RB19 solution at 30 mg/L. The equilibrium adsorption capacity (q_e), and the thermodynamic parameters including the Gibbs free energy change (ΔG^0), enthalpy change (ΔH^0), and entropy change (ΔS^0), were calculated using the van't Hoff equations.

$$\Delta G^o = -RT \ln K_c \quad (4)$$

$$\ln K_c = \frac{\Delta S^o}{R} - \frac{\Delta H^o}{RT} \quad (5)$$

where R is gas constant (8.314 J.mol^{-1}.K^{-1}), and T is the temperature (K). A plot of $\ln K_c$ versus 1/T was used to determine ΔH^o and ΔS^o.

2.6. Adsorption Isotherm Models

The equilibrium adsorption behavior of RB19 on the ZIF-67/SA/PVA composite was evaluated using the Langmuir and the Freundlich isotherm models. The linear form of the Langmuir equation is expressed as:

$$\frac{C_e}{q_e} = \frac{1}{K_L q_{\max}} + \frac{C_e}{q_{\max}} \quad (6)$$

where C_e (mg.L^{-1}) is the equilibrium concentration, q_e (mg.g^{-1}) is the equilibrium adsorption capacity, $q_{\max}$(mg.g^{-1}) is the maximum adsorption capacity, and K_L (L.mg^{-1}) is the Langmuir constant. The linear form of the Freundlich isotherm equation is given by:

$$\log\ q_e = \log\ K_F + \frac{1}{n}\log C_e \quad (7)$$

where K_F ((mg.g^{-1})(L.mg^{-1})$^{1/n}$) is the Freundlich constant and n is the heterogeneity factor of adsorption intensity.

2.7. Adsorption Kinetics

The adsorption kinetics of RB19 on the ZIF-67/SA/PVA composite were investigated using the pseudo-first-order, and pseudo-second-order models. The pseudo-first-order kinetic model is expressed in linear form as:

$$\ln\,(q_e - q_t) = \ln\ q_e - k_1 t \quad (8)$$

where q_t (mg.g^{-1}) is the adsorption capacity at time t, q_e (mg.g^{-1}) is the equilibrium adsorption capacity, and k_1 (min^{-1}) is the rate constant of the pseudo-first-order model. The pseudo-second-order kinetic model is given by:

$$\frac{t}{q_t} = \frac{1}{k_2 q_e^2} + \frac{t}{q_e} \quad (9)$$

where k_2 (g.mg^{-1}.min^{-1}) is the rate constant of the pseudo-second-order model.

3. Results and Discussion

3.1. Structural Characterization

The FTIR spectra of the SA/PVA sample exhibits a broad absorption band at ~3454 cm^{-1} belonged to –OH stretching vibrations (Figure 1). This peak indicates abundant hydroxyl groups and extensive hydrogen bonding within the polymer network. The bands at 3105 and 2914 cm^{-1} are associated with C–H stretching of –CH and $–CH_2$ groups, respectively. The band at 1764 cm^{-1} is assigned to C=O stretching of carboxyl groups in sodium alginate, and the peak at 1633 cm^{-1} is associated with asymmetric stretching of $–COO^-$ groups and/or bound water. Moreover, bands at 1384 and 1103 cm^{-1} correspond to C–O, C–N, and C–O–C vibrations, respectively. For ZIF-67, the peaks are observed in the 1350–1000 cm^{-1} region (C–N, C–O), along with aromatic and aliphatic C–H stretching bands in the 3100–2900 cm^{-1} range. In the composites, the coexistence of these characteristic bands confirms successful integration of ZIF-67 into the SA/PVA matrix. The slight shift and reduced intensity of the –OH band at 3400–3500 cm^{-1} due to hydrogen bonding interactions between polymer chains and ZIF-67 particles. Notably, ZIF-67/SA/PVA-3:1 exhibits broader –OH and C=O bands due to higher SA content. These results are consistent with previous studies on ZIF-67-based composites, in which incorporation into polymer matrices leads to band broadening and slight shifts due to interfacial interactions [20].

The XRD patterns confirm the crystalline structure of ZIF-67 and its retention within the ZIF-67/SA/PVA composites (Figure 2). Pristine ZIF-67 exhibits sharp and intense diffraction peaks at 2θ about 7.73°, 10.73°, 12.7–13.07°, 14.8°, 16.4°, 18.4°, 22.4°, and 26.7° corresponding to the (011), (002), (112), (022), (013), (222), (114), and (233) reflections, respectively. These well-defined peaks confirm the high crystallinity and successful formation of ZIF-67. The composites retain characteristic ZIF-67 reflections at 2θ ≈ 10.73°, 16.1°, 18.4°, 22.4°, and 26.55°, indicating that the framework remains crystalline after incorporation into the SA/PVA matrix. However, the reflections are less intense and broader than those of pristine ZIF-67, which can be attributed to dilution and partial masking by the amorphous polymer phase and to the dispersion of ZIF-67 particles within the matrix. This attenuation is most pronounced for ZIF-67/SA/PVA-3:1 because of the larger contribution of the SA-rich amorphous phase. In contrast, ZIF-67/SA/PVA-1:1 retains a comparatively distinct reflection at 2θ at 18.4°. Similar reductions in diffraction intensity have been reported for ZIF-67/polymer composites [21].

The SEM images reveal that the morphology of the ZIF-67/SA/PVA composites is strongly dependent on the SA/PVA ratio (Figure 3). For ZIF-67/SA/PVA-1:3, ZIF-67 particles are relatively well dispersed on the polymer surface and form a rough and porous network with visible interparticle voids. In the ZIF-67/SA/PVA-1:1 sample, the particles remain distinguishable but exhibit partial aggregation into clusters. The results indicate a moderate interaction between ZIF-67 and the polymer matrix. By contrast, the ZIF-67/SA/PVA-3:1 composite exhibits a denser and more compact surface. The ZIF-67 crystals are more tightly packed and partially embedded in the SA-rich matrix. The polyhedral morphology with relatively sharp edges is

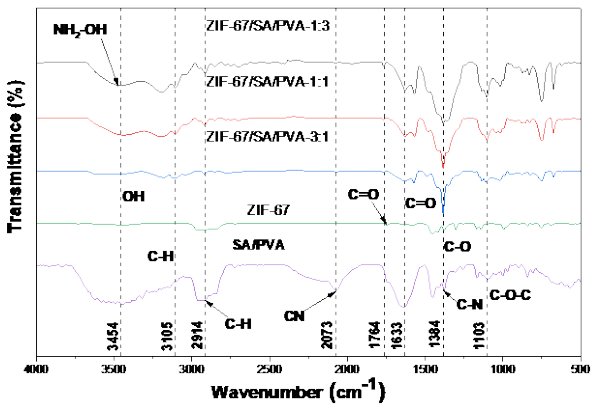

Figure 1. FTIR of composites.

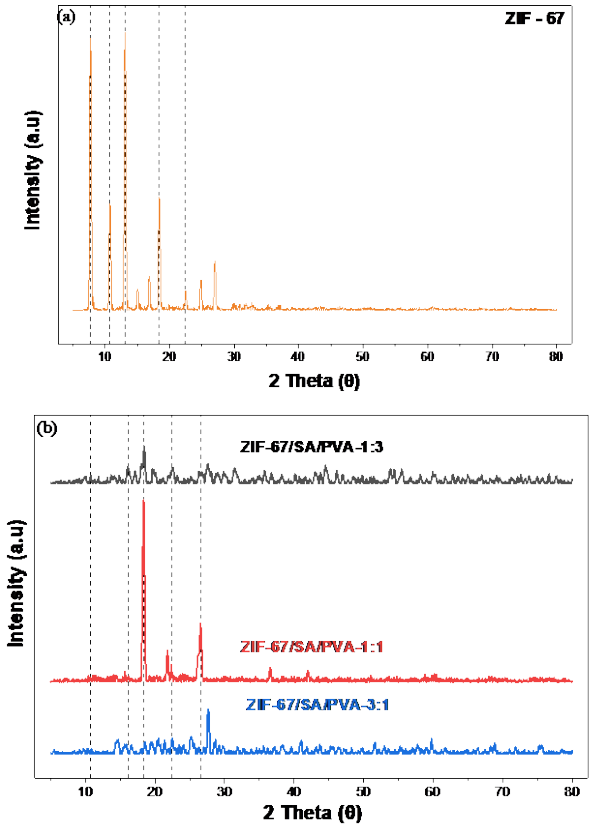

Figure 2. XRD of (a) ZIF-67 and (b) composites.

characteristic of ZIF-67 crystals and is consistent with previously reported ZIF-67-based composites [22]. EDS analysis confirms the presence of C, N, O, and Co, which are associated with the organic components and the cobalt-based framework. The Co content of approximately 3.8 wt% further supports the incorporation of ZIF-67, while the trace amount of Ca (~0.1 wt%) is attributable to alginate crosslinking (Figure 3d).

The N_2 adsorption–desorption results (Figure 4a) indicate that the ZIF-67/SA/PVA composites retain the microporous characteristics of ZIF-67, with pores mainly distributed near the micropore–mesopore boundary. All samples show a rapid N_2 uptake at low relative pressure, followed by a gradual increase as P/P_0 increases. This behavior is characteristic of a Type I adsorption isotherm

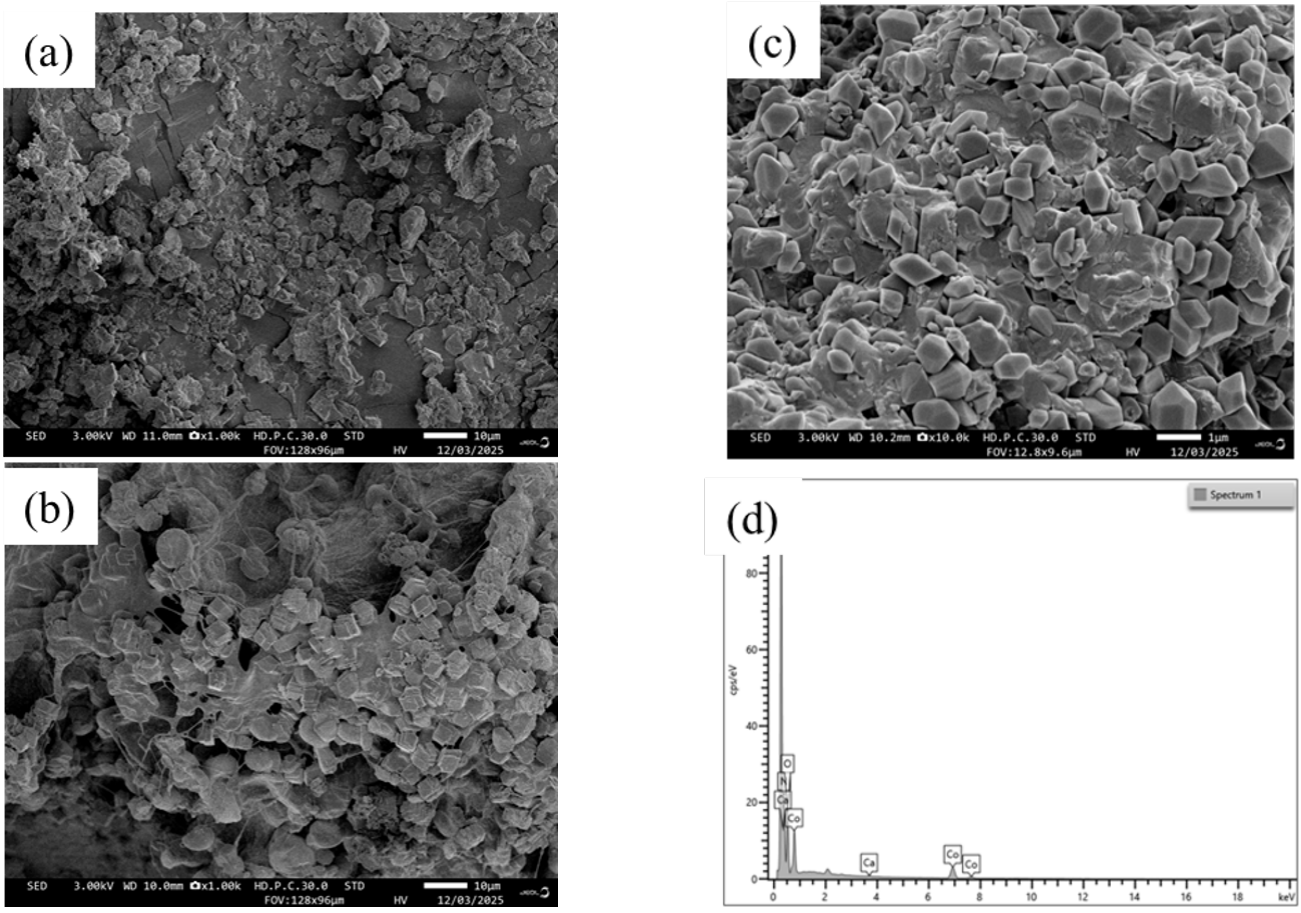

Figure 3. SEM image of (a) ZIF-67/SA/PVA-1:3, (b) ZIF-67/SA/PVA-1:1, (c) ZIF-67/SA/PVA-3:1, and (d) EDS of ZIF-67/SA/PVA-3:1.

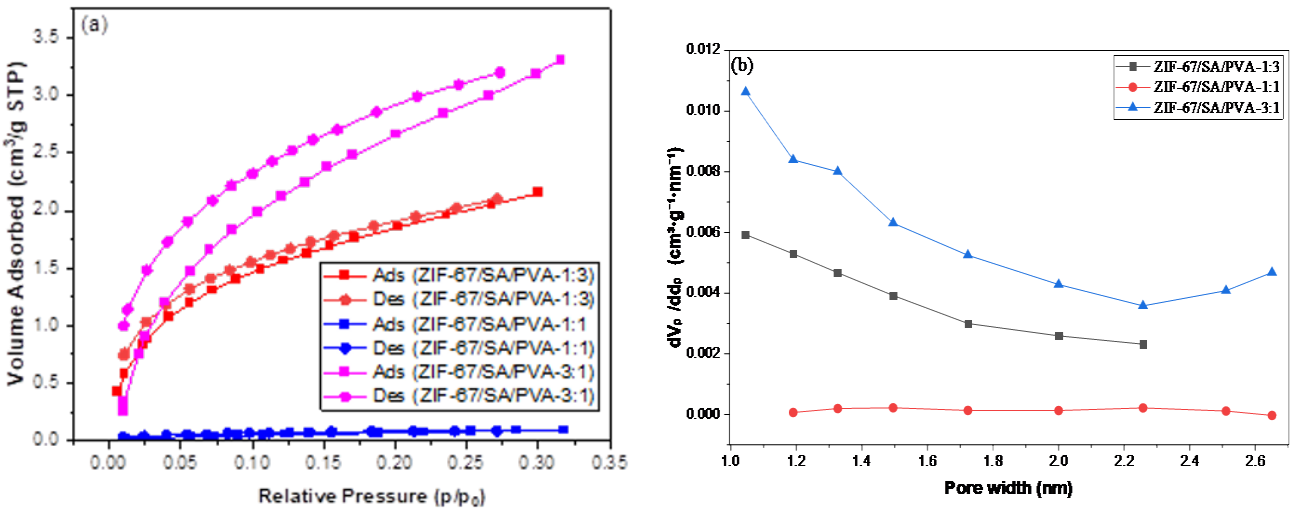

Figure 4. (a) N_2 adsorption–desorption and (b) BJH pore-size distribution of composites.

according to the IUPAC classification. A small hysteresis loop is observed for the ZIF-67/SA/PVA-1:3 and ZIF-67/SA/PVA-3:1 composites at low relative pressures, where the adsorption and desorption branches do not completely overlap. This behavior may be associated with restricted gas diffusion and structural relaxation effects within the ZIF-67/ SA/PVA polymer hybrid framework. The variation in the SA/PVA ratio clearly affects the textural characteristics of the composites. Among the investigated composites, ZIF-67/SA/PVA-3:1 exhibits the highest BET surface area (10.852 $m^2.g^{-1}$), indicating the greatest accessibility of the porous ZIF-67 framework. In contrast, ZIF-67/SA/PVA-1:1 displays a negligible BET surface area (0.3154 $m^2.g^{-1}$). The BJH pore-size distribution indicates the presence of pores near the micropore–mesopore boundary (Figure 4b). The ZIF-67/SA/PVA-3:1 exhibits the highest pore-volume distribution intensity, whereas ZIF-67/SA/PVA-1:1 displays the lowest pore-volume signal. The BET–BJH results confirm that the SA/PVA composition plays an important role in regulating the surface area accessibility and pore structure of ZIF-67/SA/PVA composites.

The thermogravimetric curves reveal the thermal stability and decomposition behavior of the ZIF-67/SA/PVA composites with different SA/PVA ratios (Figure 5a). All samples show a slight weight loss below approximately 150 °C due to the removal of physically adsorbed water and residual solvent trapped within the polymer network and pores of ZIF-67. The major weight loss occurs between 200 and 300 °C, corresponding to the thermal decomposition of the SA/PVA polymer matrix. The mass reduction was 52.36, 50.82 and 49.78% for ZIF-67/SA/PVA-3:1, ZIF-67/SA/PVA-1:1 ZIF-67/SA/PVA-1:3, respectively. Additionally, the weight loss becomes more gradual and is mainly associated with further carbonization of the polymer chains and decomposition of the organic linker in ZIF-67 at 350-500 °C with an approximate 8.9% weight loss. At higher temperatures (above 700 °C), an additional gradual weight loss of about 13.03% indicated the continued degradation of carbonaceous residues and transformation of cobalt-containing species.

The point of zero charge (pH_{pzc}) of the ZIF-67/SA/PVA composite was determined to be approximately 7.77 (Figure 5b). This value indicates that the surface charge of the composite is strongly dependent on the solution pH. When the solution pH is lower than pH_{pzc}, the material surface becomes positively charged due to protonation of surface functional groups, thereby favoring the adsorption of anionic dye molecules. In contrast, the surface becomes negatively charged due to deprotonation at pH values above 7.77. These results lead to electrostatic repulsion between the composite surface and RB19 anions and, thereby, reduce adsorption efficiency. Therefore, the pH_{pzc} result provides important evidence supporting the proposed adsorption mechanism through electrostatic interaction, hydrogen bonding and possible π–π interactions between RB19 and the ZIF-67/SA/PVA composite.

3.2 Effects of Adsorption Parameters on RB19 Removal Efficiency

The effect of SA/PVA composition on RB19 adsorption was clearly reflected in the UV–Vis spectral evolution (Figure 6). The pristine SA/PVA matrix exhibited a limited adsorption efficiency of 10.12%. In contrast, the incorporation of ZIF-67 significantly enhanced performance, with removal efficiencies increasing from 88.96% (1:1) to 92.47% (3:1) and reaching a maximum of 96.45% for ZIF-67/SA/PVA-1:3. This performance is attributed to the higher PVA content, which promotes a more flexible polymer network, and facilitates mass transfer of RB19 molecules to accessible active sites. Conversely, higher SA content may lead to a

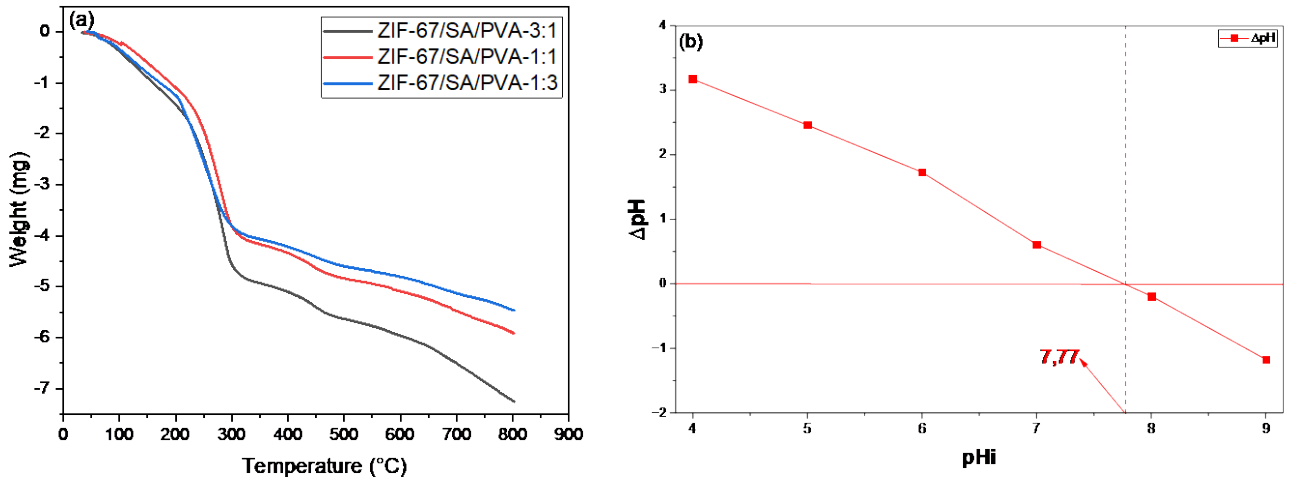

Figure 5. (a) TGA and (b) pH_{pzc} of composites.

denser gel structure due to stronger ionic crosslinking, partially limiting diffusion into the porous framework. This trend is consistent with previous reports on ZIF-67/polymer composites [23,24]. These results highlight the roles of ZIF-67 and the SA/PVA matrix, with adsorption likely governed by a combination of electrostatic interactions, hydrogen bonding, and π–π interactions between RB19 and the composite surface.

The effect of adsorbent dosage on RB19 removal is shown in Figure 7a. The adsorption efficiency increased with increasing ZIF-67/SA/PVA dosage from 0.05 to 0.20 g. At 0.05 g, the removal efficiency reached 92.53% after 300 min, while increasing the dosage to 0.075, 0.10, and 0.20 g improved the efficiency to 94.56%, 97.01%, and 99.46%, respectively. These results confirm that the amount of available adsorbent strongly influences dye removal. This enhancement can be attributed to the increased available surface area and the greater number of active adsorption sites. The higher composite dose promotes more effective contact between RB19

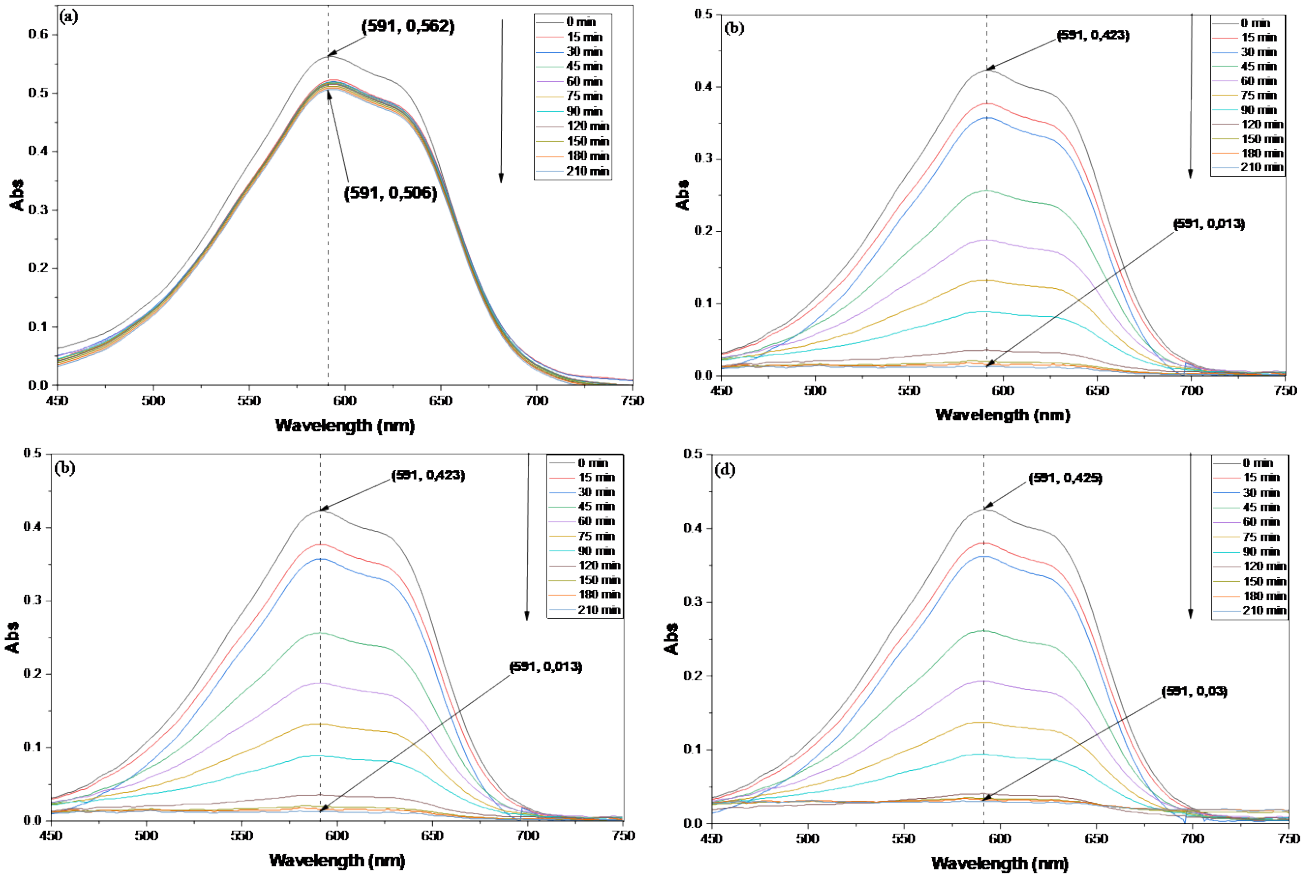

Figure 6. UV–Vis spectra of RB19 solution during adsorption using (a) SA/PVA, (b) ZIF-67/SA/PVA-1:3, (c) ZIF-67/SA/PVA-1:1, and (d) ZIF-67/SA/PVA-3:1.

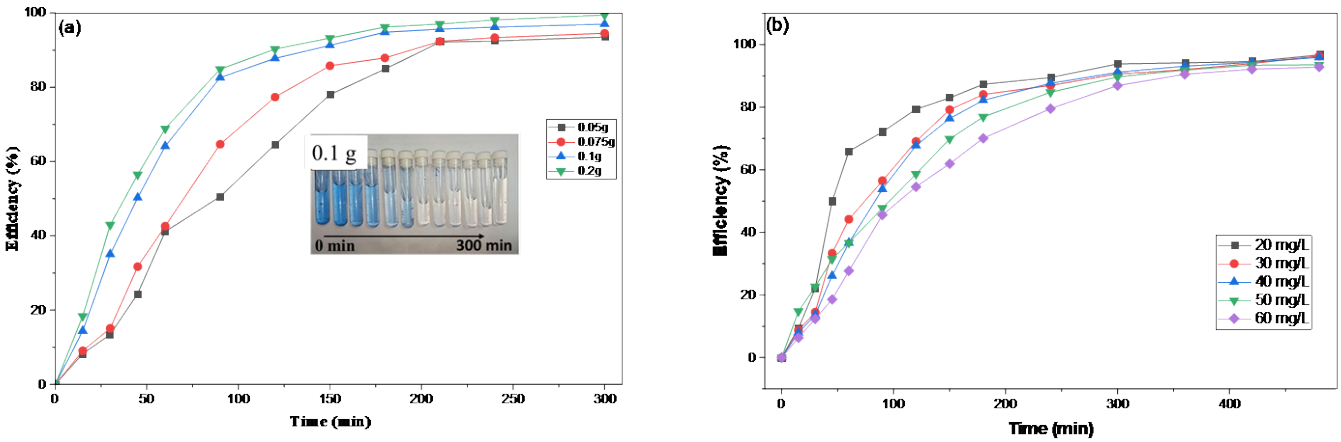

Figure 7. Effect of (a) adsorbent dosage and (b) RB19 concentration on adsorption efficiency.

molecules and the composite surface. A similar trend was reported by Amaku *et al*., who found that RB19 removal increased with increasing adsorbent dosage [25].

The effect of initial RB19 concentration on adsorption efficiency is shown in Figure 7b. The removal efficiency gradually decreased as the initial RB19 concentration increased. The highest removal efficiencies were 96.74%, 96.38%, and 95.98% at 20, 30, and 40 mg/L, respectively. However, efficiency decreased to 93.54% and 92.83% at 50 and 60 mg/L, respectively, after 480 min. This trend indicates that the available adsorption sites on the composite surface become progressively saturated at higher dye concentrations. At low RB19 concentrations, the number of active sites is sufficient for dye uptake, leading to high removal efficiency. In contrast, at high concentrations, excess RB19 molecules remain in solution because the active sites are limited and become nearly occupied. Similar behavior has been reported for RB19 adsorption onto chitin nanofiber-/nanowhisker-based hydrogels [26], and stalk/MWCNTs [25]

The effect of initial pH on RB19 adsorption can be directly explained by the pH_{pzc} of the ZIF-67/SA/PVA composite. As shown in Figure 8a, the composite exhibited high adsorption efficiency under acidic to neutral conditions, reaching 94.89% at pH of 5, 94.64% at pH of 6, and 93.43% at pH of 7. Since these pH values are lower than pH_{pzc}, the composite surface is positively charged due to protonation of surface functional groups, thereby enhancing electrostatic attraction toward anionic RB19 molecules. When the pH exceeded pH_{pzc}, the adsorption efficiency decreased to 88.64% at pH of 8 and 82% at pH of 9, which can be attributed to surface deprotonation and electrostatic repulsion between the negatively charged composite surface and RB19 anions. A similar pH-dependent adsorption behavior was reported for RB19 adsorption on magnetic sugarcane bagasse [27] and biochar [28].

The effect of temperature on RB19 adsorption is shown in Figure 8b. The adsorption efficiency increased slightly with increasing temperature. The result showed that the efficiency increased from 93.22% to 97.33% with the rise of temperature from 30-60 °C. This trend indicates that higher temperatures can promote RB19 adsorption. The improvement may be attributed to enhanced molecular mobility, reduced solution viscosity, and accelerated diffusion of RB19 molecules toward the active sites of the composite. In addition, the slight increase in adsorption efficiency at elevated temperatures suggests that the adsorption process may be endothermic.

3.3 Thermodynamic, Isotherm, and Kinetic Studies

The thermodynamic parameters for RB19 adsorption onto the ZIF-67/SA/PVA composite are summarized in Table 1. The negative values of $\Delta G°$ ranged from -5.308 kJ.mol^{-1} at 303 K to -7.298 kJ.mol^{-1} at 333 K. These results indicated that the adsorption process is spontaneous. The increasingly negative $\Delta G°$ values with increasing temperature suggest that higher temperature enhances the thermodynamic favorability of RB19 adsorption. The result is consistent with the experimental results, which show improved removal efficiency at elevated temperatures. The positive $\Delta H°$ value of 15.297 kJ.mol^{-1} indicates that the adsorption process is endothermic. This phenomenon suggests that heat facilitates the interaction between RB19 molecules and the active sites of the composite. In addition, the positive $\Delta S°$ value reflects increased randomness at the solid–liquid interface during adsorption (Table 1).

The adsorption isotherm of RB19 onto the ZIF-67/SA/PVA composite was evaluated using the Langmuir and the Freundlich models (Table 2). The Langmuir model exhibited a much better linear fit ($R^2 = 0.9903$) than the Freundlich model ($R^2 = 0.6149$). This suggests that RB19 adsorption

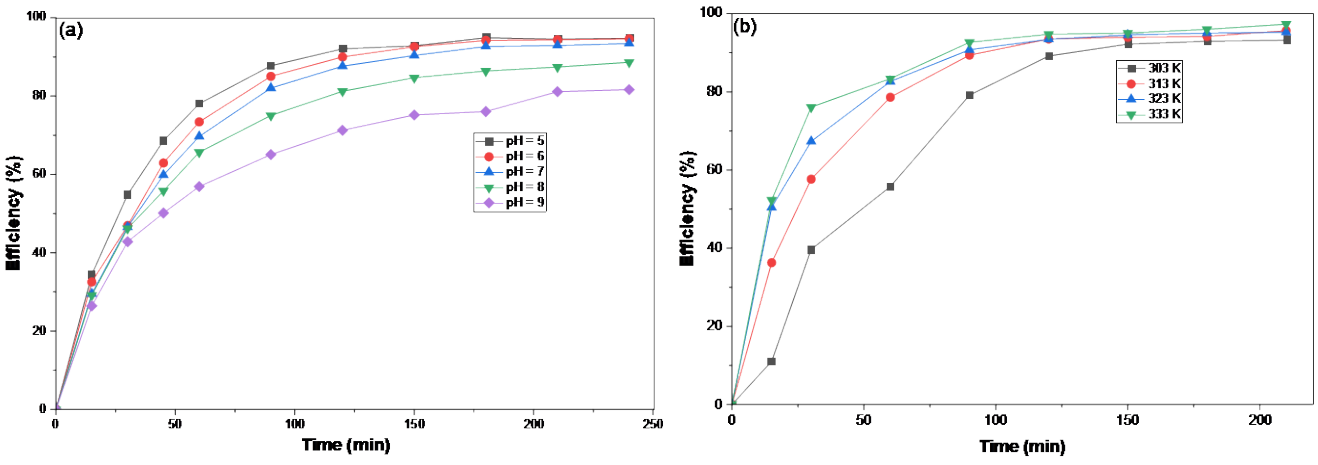

Figure 8. Effects of (a) initial solution pH and (b) temperature on RB19 adsorption efficiency.

mainly occurs as monolayer coverage on relatively homogeneous active sites of the composite surface. The maximum adsorption capacity, calculated using the Langmuir model, was 20.41 mg/g. The Langmuir constant (K_L) was 1.623 L/mg that indicated a favorable affinity between RB19 molecules and the active sites of the ZIF-67/SA/PVA composite. In contrast, the low R^2 value of the Freundlich model indicates that multilayer adsorption on a heterogeneous surface is not the dominant mechanism [29,26].

The kinetic plots and parameters provide deeper insight into the adsorption of RB19 on ZIF-67/SA/PVA. As shown in Figure 9 and Table 3, the experimental adsorption capacity increased markedly with increasing initial RB19 concentration, from 9.973 mg/g at 20 mg/L to 14.746, 19.443, 23.610, and 28.534 mg/g at 30, 40, 50, and 60 mg/L, respectively. This trend indicates that a higher initial dye concentration provides a stronger concentration gradient between the solution and the adsorbent surface. For the pseudo-first-order model, the R^2 values ranged from 0.9346 to 0.9960. The best fit was obtained at 40 mg/L with R^2 = 0.9960, suggesting that diffusion-related adsorption may be more evident at this concentration. However, the calculated adsorption capacities from the pseudo-first-order model did not consistently match the experimental values. At 20 and 30 mg/L, the theoretical q values were lower than the experimental values. However, the q value was

Table 1. The thermodynamic variables at different temperatures.

Temperature (K)	ΔG^0 (kJ mol^{-1})	ΔS^0 (kJ mol^{-1}.K^{-1})	ΔH^0 (kJ mol^{-1})
303	-5.308	0.068	15.297
313	-5.873		
323	-6.699		
333	-7.298		

Table 2. Isotherm parameters for the adsorption of RB19 onto ZIF-67/SA/PVA composite.

Model	Parameter	Value
Langmuir	q_{max} (mg/g)	20.41
	K_L (L.mg^{-1})	1.623
	R^2	0.9903
	R_L	0.01–0.03
Freundlich	K_F	10.4
	n	3.99
	1/n	0.25
	R^2	0.6149

Table 3. Kinetic parameters of pseudo-first-order and pseudo-second-order.

C_0 (mg/L)	Pseudo-first-order				Pseudo-second-order			
	k_1 (min^{-1})	$q_{e,exp}$ (mg/g)	$q_{e,cal}$ (mg/g)	R^2	k_2 (g.mg^{-1}.min^{-1})	$q_{e,exp}$ (mg/g)	$q_{e,cal}$ (mg/g)	R^2
20	0.0092	9.973	6.9054	0.9491	0.0026	9.973	10.6724	0.9995
30	0.0089	14.746	13.5204	0.9776	0.0007	14.746	17.5438	0.991
40	0.0101	19.443	21.5139	0.996	0.0003	19.443	25.7069	0.9684
50	0.0136	23.61	37.6375	0.9346	0.0002	23.61	33.3333	0.9825
60	0.0134	28.534	33.1022	0.9814	0.0001	28.534	43.6681	0.9644

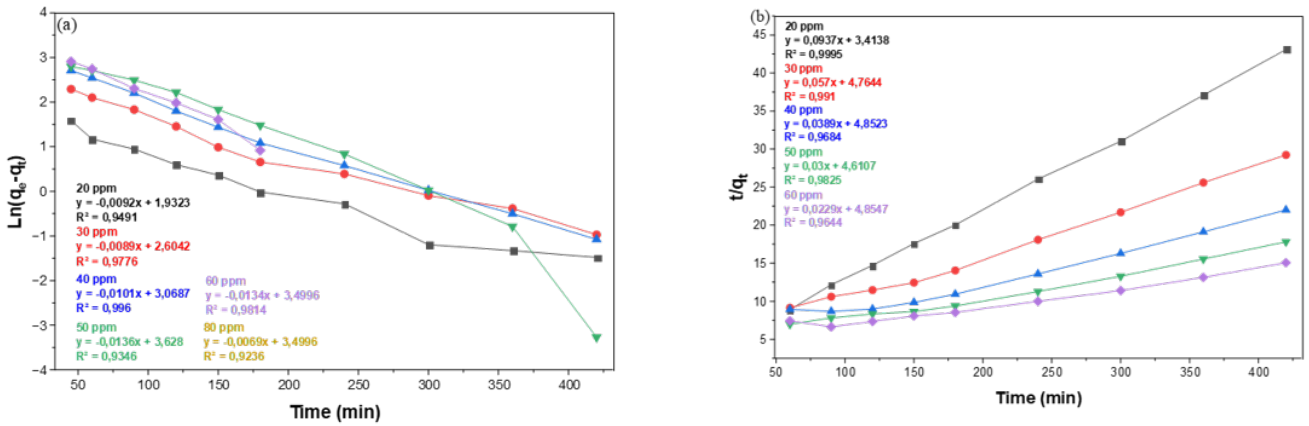

Figure 9. The (a) pseudo-first-order and (b) pseudo-second-order models.

significantly overestimated at higher concentrations (37.6375 mg/g vs. 23.610 mg/g). This deviation suggests that the pseudo-first-order model alone cannot fully describe the adsorption process over the entire concentration range. In contrast, the pseudo-second-order model gave the q values closer to the experimental data at 20 mg/L (10.6724 mg/g vs. 9.973 mg/g), but the deviation increased at higher concentrations, with q value reaching 43.6681 mg/g at 60 mg/L compared with $q_{e,exp}$ = 28.534 mg/g. Meanwhile, the pseudo-second-order rate constant decreased from 0.0026 to 0.0001 $g.mg^{-1}.min^{-1}$ as the initial RB19 concentration increased from 20 to 60 mg/L. This indicated that the adsorption rate becomes slower at higher dye loading due to progressive occupation of active sites and stronger competition among dye molecules. The contribution of electrostatic attraction, hydrogen bonding with –OH/–COO^- groups, and possible π–π interactions with the imidazolate structure of ZIF-67 likely governs the surface adsorption stage, while the reduced rate constants at higher concentrations reflect increased diffusion resistance and partial saturation of active sites.

The adsorption of RB19 onto the ZIF-67/SA/PVA composite is proposed to occur through the combined contributions of electrostatic attraction, hydrogen bonding, π–π interactions, and mass transfer through the accessible ZIF-67/SA/PVA network. Among these interactions, the pH-dependent results indicate that electrostatic attraction is a major driving force. RB19 is an anionic dye containing negatively charged sulfonate groups in aqueous solution. The pH_{pzc} of the ZIF-67/SA/PVA composite was approximately 7.77. At pH values below the pH_{pzc}, protonation of surface functional groups produces a predominantly positive surface charge. This favors electrostatic attraction between protonated sites on the composite and the –SO_3^- groups of RB19. Accordingly, the adsorption efficiency remained high at pH of 5–7 but decreased at pH of 8–9. Similar pH-dependent behavior has been reported for RB19 adsorption onto chitin-based hydrogels and biomass/MWCNT composites, for which attraction between positively charged adsorption sites and anionic sulfonate groups was identified as an important removal pathway [25,26]. Hydrogen bonding may contribute to RB19 retention. The SA/PVA matrix contains abundant hydroxyl groups, carboxylate and protonated carboxylic groups depending on solution pH. These groups can act as hydrogen-bond donors or acceptors toward the sulfonate, carbonyl, and other oxygen- or nitrogen-containing functionalities of RB19. Incorporation of ZIF-67 also introduces imidazolate nitrogen-containing surfaces and polymer–MOF interfacial sites. The shifts and broadening of the –OH-related FT-IR bands observed after composite formation support interactions between the polymer matrix and ZIF-67. Hydrogen bonding involving surface hydroxyl groups and heteroatoms of RB19 has also been proposed for other RB19 adsorbents [25]. A further contribution may arise from π–π interactions between the extended anthraquinone aromatic system of RB19 and the conjugated imidazolate rings of ZIF-67. Such interactions can enhance the affinity of aromatic dyes for ZIF-based surfaces and have previously been reported for dye adsorption onto ZIF-67-containing materials [30].

4. Conclusion

ZIF-67/SA/PVA composite beads were successfully synthesized and evaluated as adsorbents for the removal of reactive blue 19 from aqueous solution. FTIR, XRD, SEM-EDS, BET, TGA, and pH_{pzc} analyses confirmed the successful incorporation of ZIF-67 into the SA/PVA matrix. Among the investigated compositions, ZIF-67/SA/PVA-1:3 exhibited the best adsorption performance with 96.45% RB19 removal efficiency. The adsorption efficiency increased with adsorbent dosage and temperature but decreased at higher initial RB19 concentrations. The pH-dependent behavior confirmed that electrostatic attraction played an important role under acidic to neutral conditions, hydrogen bonding and possible π–π interactions. The negative $\Delta G°$ values and positive $\Delta H°$ value demonstrated that adsorption was spontaneous and endothermic. The Langmuir model described the equilibrium data more accurately than the Freundlich model, with a calculated maximum capacity of 20.41 mg/g. Kinetic analysis further showed that RB19 uptake involved both diffusion and surface-interaction processes. The findings demonstrate the potential of ZIF-67/SA/PVA composite beads as adsorbents for reactive dye removal from contaminated water.

Acknowledgment

The authors would like to thank the Industrial University of Ho Chi Minh City and Ho Chi Minh City University of Industry and Trade for facilities support.

CRedit Author Statement

Author Contributions: Methodology and formal analysis (Nguyen Thi Hong Nhung); Methodology (Pham Thi Huynh Nhu); Data curation (Hoang Ai Le Pham); Investigation, Writing - Review and Editing (Thi Hong Anh Nguyen). All authors have read and agreed to the published version of the manuscript.

References

[1] Al-Tohamy, R., Ali, S.S., Li, F., Okasha, K.M., Mahmoud, Y.A.-G., Elsamahy, T., Jiao, H., Fu, Y., Sun, J. (2022). A critical review on the treatment of dye-containing wastewater: Ecotoxicological and health concerns of textile dyes and possible remediation approaches for environmental safety. *Ecotoxicology and Environmental Safety*, 231, 113160. DOI: 10.1016/j.ecoenv.2021.113160.

[2] Fadzli, J., Hamid, K.H.K., Him, N.R.N., Puasa, S.W. (2022). A critical review on the treatment of reactive dye wastewater. *Desalination and Water Treatment*, 257, 185–203. DOI: 10.5004/dwt.2022.28028.

[3] Mustafa, G., Younas, A., Zahid, M.T., Kim, D.-W., Jamil, I., Yadav, N., Kurade, M.B., Saha, S., Yadav, K.K., Jeon, B.-H. (2025). Bioremediation of reactive blue 19 dye by laccase-producing Serratia marcescens AY4 strain. *Journal of Environmental Chemical Engineering*, 13(2), 115605. DOI: 10.1016/j.jece.2025.115605.

[4] Satyam, S., Patra, S. (2024). Innovations and challenges in adsorption-based wastewater remediation: A comprehensive review. *Heliyon*, 10(9), e29573. DOI: 10.1016/j.heliyon.2024.e29573.

[5] Zheng, D., Wang, K., Bai, B. (2024). A critical review of sodium alginate-based composites in water treatment. *Carbohydrate Polymers*, 331, 121850. DOI: 10.1016/j.carbpol.2024.121850.

[6] Zhao, S., Li, D., Cai, Y., Wang, Y., Ling, Y., Song, Z., Liu, H. (2025). Facile synthesis of sodium alginate-polyethyleneimine aerogel and its efficient sequential adsorption toward phytic acid and copper ions. *Separation and Purification Technology*, 378, 134603. DOI: 10.1016/j.seppur.2025.134603.

[7] Wang, W., Huang, Y., Pan, Y., Dabbour, M., Dai, C., Zhou, M., He, R. (2025). Sodium Alginate Modifications: A Critical Review of Current Strategies and Emerging Applications. *Foods*, 14(22), 3931. DOI: 10.3390/foods14223931.

[8] Ahmad Raus, R., Wan Nawawi, W.M.F., Nasaruddin, R.R. (2021). Alginate and alginate composites for biomedical applications. *Asian Journal of Pharmaceutical Sciences*, 16(3), 280–306. DOI: 10.1016/j.ajps.2020.10.001.

[9] Thanh, N.D., Thi, N.T., Nguyen, V.C., Pham, H.A. Le (2026). Facile Fabrication of Alginate–BiBDC Composite Beads for Efficient Removal of Methylene Blue from Aqueous Solutions. *Bulletin of Chemical Reaction Engineering & Catalysis*, 21(3), 539–552. DOI: 10.9767/bcrec.20680.

[10] Mihai, M., Lotos, E.-D., Zaharia, M.-M., Bucatariu, F., Vasiliu, A.-L. (2024). Alginate-based Composite Hydrogels Formed by In Situ $CaCO_3$ Crystallization. *Crystal Growth & Design*, 24(6), 2514–2525. DOI: 10.1021/acs.cgd.3c01518.

[11] Vinceković, M., Živković, L., Turkeyeva, E., Mutaliyeva, B., Madybekova, G., Šegota, S., Šijaković Vujičić, N., Pustak, A., Jurkin, T., Kiš, M., Kajić, S. (2024). Development of Alginate Composite Microparticles for Encapsulation of Bifidobacterium animalis subsp. lactis. *Gels*, 10(11), 752. DOI: 10.3390/gels10110752.

[12] Lam, W.H., Tee, L.H., Ban, Z.H. (2024). A Facile and Rapid Immobilization Method of Titanium Dioxide-Alginate Composite for The Photocatalytic Removal of Reactive Black-5. *Bulletin of Chemical Reaction Engineering & Catalysis*, 19(2), 230–241. DOI: 10.9767/bcrec.20133.

[13] Daud, N.K., Abdullah, H., Ismail, N.A. (2026). Comparative Evaluation of Fe-MOF, Cu-MOF, and Bimetallic Fe/Cu-MOF for Enhanced CO_2 Adsorption: Synthesis, Characterization, and Performance Analysis. *Bulletin of Chemical Reaction Engineering & Catalysis*, 21(2), 452–466. DOI: 10.9767/bcrec.20658.

[14] Sun, C., Wang, Y., Chang, Z., Ma, Z., Yao, W., Chen, Z. (2026). Tailoring metal-organic frameworks for water decontamination: From pore structure engineering to mechanistic insights. *Journal of Environmental Chemical Engineering*, 14(3), 122673. DOI: 10.1016/j.jece.2026.122673.

[15] Zeggai, F. zohra, Ait-Touchente, Z., Bachari, K., Elaissari, A. (2025). Investigation of Metal-Organic Frameworks (MOFs): Synthesis, Properties, and Applications - An In-Depth Review. *Chemical Physics Impact*, 10, 100864. DOI: 10.1016/j.chphi.2025.100864.

[16] Mala, F.S., Saridewi, N., Nurbayti, S., Adawiah, A., Zulys, A. (2026). Synthesis of Cu-PTC (Perylene 3,4,9,10-tetracarboxylate) Metal-Organic Framework (MOF) for Methylene Blue Photodegradation. *Bulletin of Chemical Reaction Engineering & Catalysis*, 21(2), 262–273. DOI: 10.9767/bcrec.20525.

[17] Nachaichot, A., Phonlakan, K., Nijpanich, S., Pornsuwan, S., Budsombat, S. (2024). Zeolitic imidazolate framework-67 in chitosan-grafted hydrogel as an effective catalyst for peroxymonosulfate activation to degrade antibiotics and dyes. *RSC Advances*, 14(48), 35628–35637. DOI: 10.1039/D4RA06537A.

[18] Zhao, Y., Chang, Y., Li, R., Zhang, T., Xu, C., Sun, P., Liang, L., Li, Y. (2026). Biochar–Cellulose–Sodium Alginate Composite Hydrogel (BCSA) for Methylene Blue Removal: Performance Evaluation and Mechanistic Investigation. *ACS Omega*, 11(11), 17315–17328. DOI: 10.1021/acsomega.5c09986.

[19] Mustapha, L.S., Emmanuel, S.S., Obayomi, O.V., Yusuff, A.S., Tan, I.S., Lau, S.Y., Zhang, J., Obayomi, K.S. (2026). Recent advances in MOF-based composites engineered for dyes and metal ions removal from aqueous environments. A review. *Microporous and Mesoporous Materials*, 407, 114108. DOI: 10.1016/j.micromeso.2026.114108.

[20] Zhang, X., Li, Z., Zhang, T., Chen, J., Ji, W., Wei, Y. (2022). Fabrication of sodium alginate-melamine@ZIF-67 composite hydrogel and its adsorption application for Pb(II) in wastewater. *Environmental Science and Pollution Research*, 30(7), 18364–18379. DOI: 10.1007/s11356-022-23072-y.

[21] Hammi, N., Couzon, N., Loiseau, T., Volkringer, C., El Kadib, A., Royer, S., Dhainaut, J. (2023). Hierarchically porous ZIF-67/chitosan beads with high surface area and strengthened mechanical properties: Application to CO2 storage. *Materials Today Sustainability*, 22, 100394. DOI: 10.1016/j.mtsust.2023.100394.

[22] Yuan, J., Lin, Y., Huo, S., Zhang, W., Yao, K., Ma, M., Pan, Y.-T. (2026). ZIF-67-driven synergistic strategies for high-performance flame retardant polymer nanocomposites. *Advanced Nanocomposites*, 3, 261–277. DOI: 10.1016/j.adna.2026.02.004.

[23] Zhao, Y., Yuan, N., Bian, D., Sun, J., Qian, G. (2024). Preparation of a novel CSM@ZIF-67 composite microsphere to facilitate Congo red adsorption from dyeing wastewater. *Environmental Technology*, 45(11), 2255–2267. DOI: 10.1080/09593330.2023.2169640.

[24] Zhu, K., Mohammed, S., Tang, H., Xie, Z., Fang, S., Liu, S. (2023). ZIF-67/SA@PVDF Ultrafiltration Membrane with Simultaneous Adsorption and Catalytic Oxidation for Dyes. *Sustainability*, 15(4), 2879. DOI: 10.3390/su15042879.

[25] Amaku, J.F., Taziwa, R. (2024). Removal of reactive blue 19 from simulated wastewater using Solanum melongena stalk/MWCNTs: thermodynamics, kinetic, equilibrium and regeneration potentials. *Chemical Papers*, 78(2), 1251–1263. DOI: 10.1007/s11696-023-03163-x.

[26] Liu, L., Wang, R., Yu, J., Hu, L., Wang, Z., Fan, Y. (2018). Adsorption of Reactive Blue 19 from aqueous solution by chitin nanofiber-/nanowhisker-based hydrogels. *RSC Advances*, 8(28), 15804–15812. DOI: 10.1039/C8RA01563E.

[27] Vu, T.T.H., Bui, T.D., Nguyen, L.H.K., Nguyen, T.H.A. (2025). Polyethyleneimine-Functionalized Magnetic Bagasse Composite for Efficient Adsorptive Removal of Yellow 4GL and Black R–S Dyes. *Bulletin of Chemical Reaction Engineering & Catalysis*, 20(2), 318–330. DOI: 10.9767/bcrec.20368.

[28] Rajagopalan, V.S., Rajendran, Y., Lakshumiah, A., Ravindiran, G. (2022). Batch, thermodynamic, and regeneration studies of Reactive Blue 19 using Ulva reticulata (biochar). *Desalination and Water Treatment*, 267, 231–239. DOI: 10.5004/dwt.2022.28667.

[29] Kola, D.Y., Edebali, S. (2025). Facile synthesis of zeolitic-imidazole framework-67 (ZIF-67) for the adsorption of indigo carmine dye. *The Canadian Journal of Chemical Engineering*, 103(5), 2373–2385. DOI: 10.1002/cjce.25503.

[30] Liu, L., Wang, R., Yu, J., Hu, L., Wang, Z., Fan, Y. (2018). Adsorption of Reactive Blue 19 from aqueous solution by chitin nanofiber-/nanowhisker-based hydrogels. *RSC Advances*, 8(28), 15804–15812. DOI: 10.1039/C8RA01563E.